PAPER

Limit of incorporating cesium cations into formamidinium-methylammonium based mixed halide perovskite solar cells

IOP Publishing Nanotechnology
Nanotechnology 31 (2020) 135406 (8pp) https://doi.org/10.1088/1361-6528/ab6230

Limit of incorporating cesium cations into formamidinium-methylammonium based mixed halide perovskite solar cells

Pravakar P Rajbhandari and Tara P Dhakal

Center for Autonomous Solar Power (CASP), and Department of Electrical and Computer Engineering, Binghamton University, Binghamton, NY 13902, United States of America

E-mail: tdhakal@binghamton.edu

Received 17 July 2019, revised 27 October 2019
Accepted for publication 16 December 2019
Published 15 January 2020

Abstract

Incorporating formamidinium (FA) into methylammonium (MA) based perovskite has brought significant thermal and environmental stability including best device performance. It has been shown that addition of Cesium (Cs) makes perovskite robust in terms of thermodynamic stability as well. We explore the means of incorporating Cs into a base perovskite of mixed cation (FA/MA) and mixed halide (I/Br) that has a proven track record of high performance through an inter-diffusion approach. With this approach, it has been shown that perovskites form a smooth film without any residual PbI_2 and exhibit higher absorbance. Though the residual PbI_2 disappeared with the increase in added Cs, the film morphology became rough for Cs concentration higher than 15%. Addition of small amounts of $PbCl_2$ allowed inclusion of more Cs content, which resulted in smooth film surface and further improved device performance.

Supplementary material for this article is available online

Keywords: perovskite, thin-film solar cells, Cs-incorporation, inter-diffusion, mixed-cations, two-step process

(Some figures may appear in colour only in the online journal)

1. Introduction

The power conversion efficiency of perovskite solar cells (PSC) has reached beyond 22%, propelling it toward commercialization due to its low manufacturing cost [1–3]. However, there is still room for improvement as the theoretical limit is beyond 30% depending on the bandgap [4, 5]. Although the efficiency of PSCs is impressive, the stability is still a prime concern [6]. Various device architectures, absorber compositions and deposition processes, have been investigated for stable and efficient PSCs [7–11].

The p–i–n architecture (inverted structure) wherein the absorber is sandwiched between hole and electron transport layers (ETL) has attracted many researchers mainly due to its ease of fabrication [12, 13]. There is a wide availability of ETL compared to that of hole transport layers (HTL) that are suitable for PSCs [14]. Because of the limited choice of HTLs, the inverted structure is suitable as it provides higher degree of freedom in coating processes of HTLs before the perovskite layer is placed. Additionally, the inverted structure is an excellent choice for multijunction solar cells [14–16]. Though initial inverted devices suffered from low open circuit voltage (V_{OC}), it has been shown recently to be greater than 1.2 V with suitable transport layers and surface passivation [12].

An inorganic-organic hybrid perovskite crystalizes in the form ABX_3, where A is organic and/or inorganic large monovalent cation, B is smaller divalent metal cation such as Pb^{2+}, Sn^{2+} or Ge^{2+} and X is any combination of halide ions that bond to both A and B. Varying the halides used for X alters the bandgap of the material, and it has also been reported that the smaller ionic radius for X favors the formation of cubic structure with the widely used Goldschmidt tolerance factor essential for photovoltaic performance [17]. The overall combination of A, B and X leads to distinct electro-optical properties with different level of structural

stability. The Goldschmidt tolerance factor predicts the stability of such structure based on its chemical formula ABX_3, and the ionic radii of each ions [7]. In this structure, the size of A is critical to the formation of a stable close-packed structure. Methylammonium (MA) is the most widely studied cation for perovskites, but other alternatives are employed because of its inherent instability towards moisture, heat and light. Formamidinium (FA), one of the popular alternatives, based perovskites have been studied because of its lower bandgap (closer to ideal for single junction) and better photo stability than MA-based perovskites [18]. A particular challenge is that a phase of photo-inactive—yellow $FAPbI_3$ polymorph (δ-phase, hexagonal structure) is stable at ambient pressure and room temperature, whereas the desired photoactive phase—black perovskite (α-phase, trigonal structure) is stable at temperatures above 160 °C. Fortunately, the α-phase $FAPbI_3$ perovskite that is stable at room temperature can be achieved by adding a small amount of $MAPbBr_3$ to it [19]. For more robust thermodynamic stability, an inorganic cation replacement such as with Cs and Rb has shown promise [20, 21]. In its pure form, $CsPbI_3$ has a large bandgap (~1.73 eV) which is not suitable for single cell PV application and is also unstable in photoactive α-phase in ambient atmosphere. However, a proper mix of cations and/or halides has been shown to enhance the performance and stability [2, 19, 22, 23].

It has been suggested that an inter-diffusion based deposition, commonly called 2-step process, could suppress the formation of interstitial iodide, leading to low defect densities that can be achieved from wider distribution of deposition conditions, in comparison to single step approach [24]. In the two-step process, the synthesis of perovskite is carried out through the inter-diffusion of the second precursor into the first precursor. Organohalide perovskite films deposited using two-step method exhibit improved uniformity and reproducibility because they do not have to deal with high concentrations of iodoplumbates during film formation [24]. The inter-diffusion process is also applicable to substrate with rough surface or with texture. If the first step of the fabrication is achieved conformally (e.g. by vapor deposition) on the surface topography, it allows the overall perovskite to form conformally on the surface irrespective of how the second step is performed. This technique has shown excellent results in tandem solar cell where perovskite is deposited over textured silicon bottom cell [16].

In this study, we begin with a base configuration of $FA_{0.83}MA_{0.17}Pb(I_{0.83}Br_{0.17})_3$ which has been shown as an efficient absorber [3, 18, 19] and attempt to incorporate Cs ions into it. Previous studies has been done in forming mixed cation halide perovskite to explore its feasibility [25–29]. For an inverted planar PSC, we explore the limit of incorporating Cs ions using inter-diffusion based approach for the fabrication of high-quality triple-cation perovskite.

2. Experimental section

2.1. Materials

The nickel nitrate hexahydrate, ethylene glycol, ethylenediamine, chlorobenzene, N,N-dimethylformamide (DMF), dimethyl sulfoxide (DMSO) and anhydrous 2-propyl alcohol were purchased from Sigma-Aldrich. PCBM was purchased from nano-C. FAI and MABr were purchased from Great Solar. CsI was purchased from Alfa Aesar. PbI_2 and $PbBr_2$ were purchased from TCI. Atomic layer deposition (ALD) precursor Dimethyl Zinc (DMZ) was purchased from STREM chemicals.

2.2. Device fabrication

ITO glass purchased from University Wafers (~7 Ω/□) was washed with detergent and sonicated in acetone and 2-propanol in sequence and then blow dried with nitrogen. Just before use, the ITO glass was further exposed to UV-ozone in oxygen rich atmosphere for 15 min. Then, the substrate was spin coated with a 1 M mixture of nickel nitrate hexahydrate and ethylene diamine in ethylene glycol at 6000 rpm for 60 s. The substrate was then annealed in ambient air at 300 °C for 60 min. This process resulted with NiO film of ~20 nm. The sample was then moved to a glovebox for the coating of perovskite absorber. For the first step a mixture 1.3 M of PbI_2, $PbBr_2$, ($PbCl_2$ in some cases) and CsI in a solvent mixture of DMF:DMSO in 4:1 vol/vol ratio was spin coated on to the NiO_x coated substrate statically at 3000 rpm for 40 s and dried on its own for couple of minutes or on a hotplate at 50 °C for 1 min. In the second step a mixture of FAI (80 mg) and MABr (10 mg) in 1 ml of anhydrous 2-propanol was dynamically casted on the substrate at 5000 rpm for 30 s. The sample is light brown in color when taken off the spin coater and is dried at room temperature. In 4 to 5 min, the sample looks dark brown in color after which it was placed in the hot plate and annealed at 140 °C for 15 min giving a high-quality perovskite film of ~ 420 nm. After cooling down, 17 mg ml^{-1} PCBM in chlorobenzene is spin coated statically from a 0.45 μm syringe filter at 2000 rpm for 40 s and annealed at 75 °C for 2 min, which resulted in ~ 40 nm thick PCBM layer. Then, the sample was taken out of the glovebox and any further processing and characterization were performed in ambient air. A buffer layer of ZnO (2 nm—10 cycles) is grown in an ALD reactor from the precursors such as DMZ and water (H_2O) at 100 °C. Then an 80 nm thick silver (Ag) top electrode is deposited in a thermal evaporator using a shadow mask of sizes of 0.09 cm^2 and 0.04 cm^2. Thus the device structure was glass/ITO/NiO_x/Cs:$FA_{0.83}MA_{0.17}Pb(I_{0.83}Br_{0.17})_3$/PCBM/ZnO/Ag. The schematic of fabrication process is shown in figure 1.

2.3. Characterization

The structural and phase characterization of perovskite is performed with x-ray diffraction (XRD) on a PanAnalytical X'Pert PRO x-ray diffraction system which uses CuKα x-rays

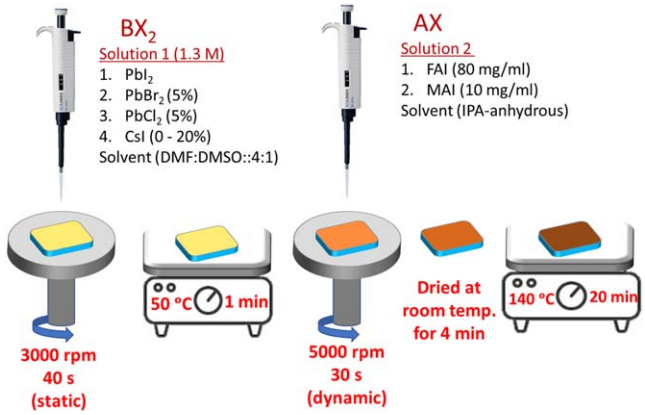

Figure 1. Fabrication process for the perovskite thin film.

and line-focus optics. Carl Zeiss supra 55 VP—high resolution—scanning electron microscope (HR-SEM) was used to study the morphology of the films. The photoluminescence (PL) was measured using Horiba's PL measurement system with 532 nm laser and photo multiplier tube (PMT) detector. Absorbance was measured using the Ångstrom Sun Technologies' TF Probe UV/Vis spectrophotometer. IV characterization was carried out using Keithley's 4200-SCS semiconductor characterization system along with the solar simulator from Photo Emission Tech. External quantum efficiency (EQE) was measured using Solar Cell Spectral Response Measurement System from PV Measurements.

3. Results and discussion

The first precursor (from here on called S1-precursor) was composed of PbI_2 mixed with 5% $PbBr_2$ in DMF:DMSO in 4:1 vol/vol ratio, while the second precursor (from here on called S2-precursor) was composed of MABr & FAI in 2-propanol. The inter-diffusion of the S2-precursor into the S1-precursor film poses a challenge in converting all the S1-precursor into the perovskite phase. The weak interlayer bonding in PbI_2 allows a rapid intercalation of a new cation into the crystal but increasing thickness of PbI_2 layer makes inter-diffusion more difficult, leaving behind some unconverted PbI_2 [30]. However, multiple reports mention that residual PbI_2 aids in passivating the grain boundaries [31–35]. For the two-step process to yield a high-quality perovskite film, both the steps are equally important. The first step needs to make a compact and uniform layer of S1-precursor and the second step should convert it to a high-quality perovskite film.

3.1. Mitigation of rough texture during fabrication procedure

For the first step, pure dimethylformamide (DMF) is commonly used as a solvent but it dries very quickly and forms a rough surface. To slow down the drying process dimethyl sulfoxide (DMSO) with higher boiling point (B.P. 189 °C) is added to the solvent in the volume ratio of 4(DMF):1(DMSO) [36]. In our observation, the duration of spin speed severely affected the roughness of the film from the first step. If it is spun for less than 30 s, the S1-precursor dried creating surface that appeared rough and frosty. However, when they were spun for more than a minute, it resulted in a mirror smooth film. This happens because a longer spin will allow the DMF in the precursor to completely dry while less volatile DMSO remains in the film and evaporates slowly at room temperature to prevent the film from becoming rough.

Application of the second step solution prior to drying the S1-precursor resulted in the films turning dark-brown instantly. This means the film converted to perovskite phase at room temperature during spinning, but with a rough texture. To get a smooth perovskite film, the DMF needs to evaporate from the S1-precursor before applying the second step solution. We tried a hypothesis that if we apply diethyl ether (which is a unique solvent that dissolves DMF but not DMSO) during spinning of S1-precursor, it should result in S1-precursor with only DMSO left creating a PbI_2-DMSO complex. However, the results were not very repeatable as it still needed some time for drying afterwards. This would mean that not only DMF needs to be out of the film, the film itself needs to be dry because the reaction will be very fast in liquid state than in dried-solid state.

In the second step, we dispensed a fixed volume of solution at a dynamic speed for a fixed duration. We observed that no matter the quantity of S2-precursor used, some PbI_2 remained unconverted at the bottom for the films without Cs. These results were verified by doing x-ray diffraction of the thin films fabricated with varying amount of S2-precursor which is shown in figure SI_1 of the supplementary information (SI) document available online at stacks.iop.org/NANO/31/135406/mmedia.

3.2. Cs-enhanced inter-diffusion

For the mixed cation two-step perovskite fabrication process, it is common to have BX_2 such as PbI_2 in first step and AX such as the mixed cation MABr & FAI in second step for any combination of ABX_3. The solubility of Cesium Iodide (CsI) is very low in the S2-precursor solvent (2-propanol). Therefore, it was added into the S1-precursor. With the application of S2-precursor onto the S1-precursor film containing CsI, the resulting perovskite turned darker in color during the spinning process even without any annealing. This phenomenon suggests that a small portion of CsI in the first step created a spread of perovskite phase-$CsPbI_3$ within BX_2's lattice sites such that S2-precursor that followed could diffuse deeper into the film from the first step (see figures 1 and 2). This process is analogous to the one in inter-molecular exchange reported earlier [37] where a PbI_2:DMSO complex formed in first step is already a perovskite phase so that it does not have to undergo a big structural change during the inter-diffusion of the S2-precursor. This approach of adding AX such as CsI in the 1st step is also reported earlier for single cation based perovskite ($MAPbI_3$), where it was shown to provide controlled deposition via adjustable volume expansion [28] and for double cation based perovskite of Cs and FA [25–27] on n–i–p architecture.

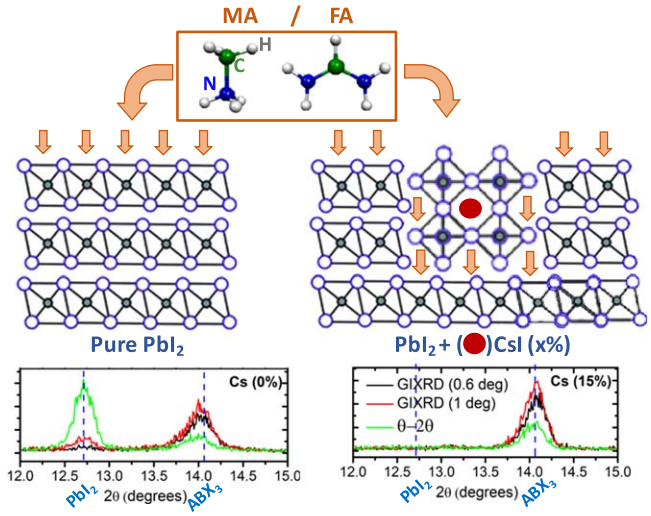

Figure 2. Overall graphics view of the formation of perovskite phase after Cs-incorporation. Top view shows the structural transformation and the bottom view shows XRD peak of pure perovskite (ABX_3) phase after Cs-inclusion.

3.3. Removal of residual PbI_2

To see the effect of Cs on the residual PbI_2, Grazing Incidence x-ray Diffraction (GIXRD) with the incidence angle of 0.6° was performed to see the phases on the surface. Another set with a greater angle of incidence at 1.0° was performed to see the phase into the bulk/deeper region of the perovskite. And a normal XRD (θ–2θ) was performed to probe all the way into the film. We can see from figure 3 that the PbI_2 peak not only decreases with the increase in Cs concentration at the surface but was completely absent from θ–2θ scan for 15% Cs concentration suggesting removal of most of, if not all, the residual PbI_2.

3.4. Optical properties of the film

The addition of Cs cation in the first step helped increase the absorbance of the perovskite. It is mostly because more of the S1-precursor was converted to perovskite phase. This was clearly seen from the absorbance spectroscopy in figure 4. The absorbance for Cs = 15% is increased both before and after the bandgap transition. The increase in absorbance for energy higher than bandgap is likely due to increased rough surface (as understood from frosty films seen in figure 6 for higher Cs-concentration) that contributed to more diffusive reflection. As expected the absorption coefficient (α) of the perovskite film, which was calculated by dividing the absorbance by the thickness of the film, increased as the absorbance increased. The highest α calculated at 600 nm was $3.4 \times 10^4\ cm^{-1}$ for the film with 15% Cs.

The photoluminescence (PL) data is similar to data previously reported [1]. The PL intensity is highest for the sample with highest amount of residual PbI_2 and then it gradually decreased with the decrease in PbI_2 content as shown in figure 5. This shows that PbI_2 passivates grain boundaries, reducing the recombination loss and thus improving the PL. Additionally, with the added Cs from 0%

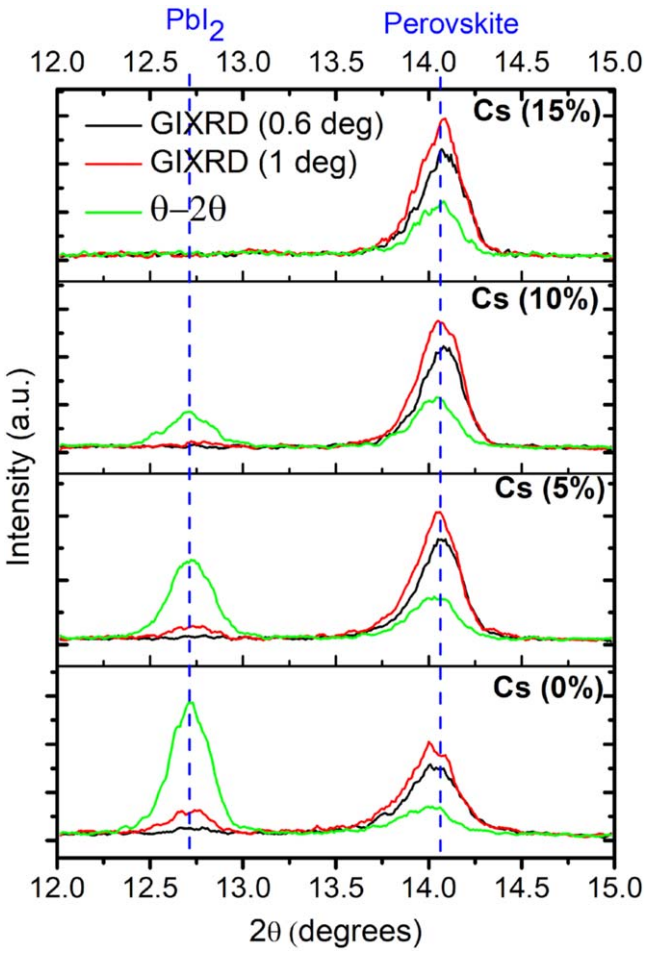

Figure 3. XRD of perovskite with different concentration of Cs performed with grazing incidence at 0.6°, 1.0° and a normal θ –2θ scan.

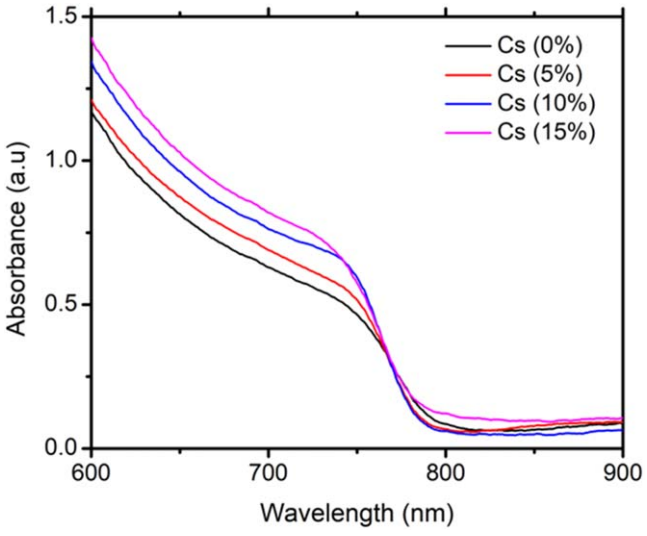

Figure 4. Absorbance spectroscopy of the perovskite film with varying Cs concentration.

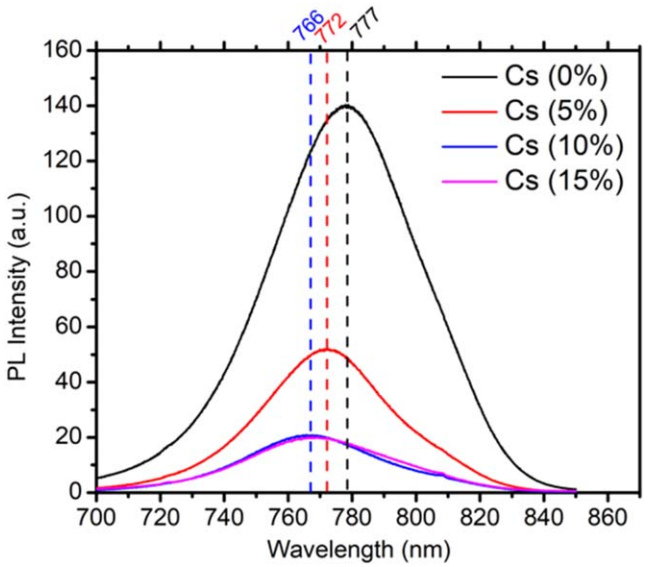

Figure 5. Photoluminescence spectra of perovskites with different concentration of Cs.

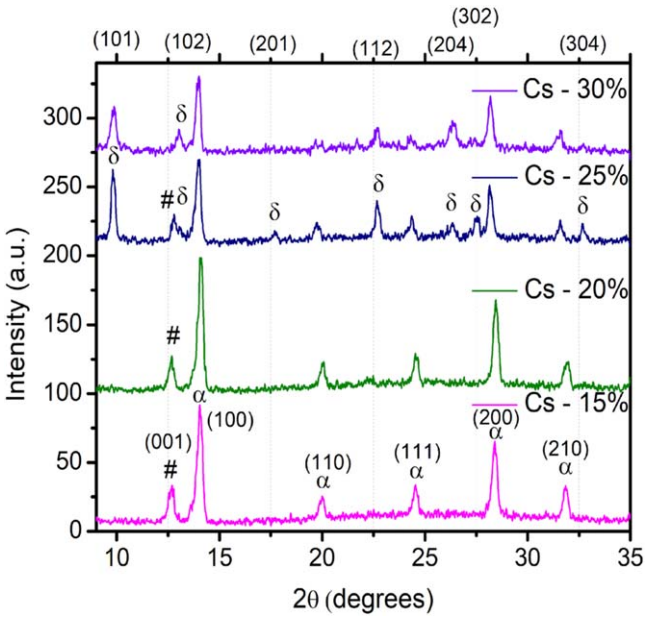

Figure 7. XRD of perovskite with a range of Cs incorporation from 15% to 30% fabricated with the process in which films are annealed after Step 1 spin coating. (#—PbI_2, α—perovskite phase (cubic), δ—non-perovskite phase (orthorhombic)).

to 15% the PL peak blue-shifts about ~11 nm, similar to what is previously reported [23].

3.5. Surface morphology

As seen from SEM image in figure 6, the films with up to 10% Cs are smooth with grain size ranging from 100 to 300 nm. In contrast, the SEM images for perovskite with 15% Cs show rough texture on top surface with bright features. Since the surface XRD for the sample does not show any PbI_2 phases (figure 3), the white features that is seen are extra FAI and/or MABr left from the 2nd spinning step which was verified by Energy-dispersive x-ray spectroscopy (EDS) with relatively higher concentration of N_2 on the bright spot.

3.6. Limit of Cs incorporation

With the current process, Cs can be added up to 10% without any side effects. Addition of $PbCl_2$ in the 1st step solution allowed to incorporate more Cesium into perovskite without the adverse effect in the surface morphology. Transmission spectroscopy showed a clear difference in absorption for the 15% Cs film with and without $PbCl_2$ as seen in figure SI_2. The film with $PbCl_2$ showed improved transmittance, indicating the frostiness shown in figure 6 with 15% Cs was removed or minimized by the addition of $PbCl_2$. The addition of $PbCl_2$ apparently allowed more Cs inclusion, however the perovskite film started to turn light brown at 25% and orange with 30% cesium, indicating a conversion into an orthorhombic phase. The XRD for the conversion to orthorhombic phase is shown in figure 7, which is also supported by huge red shift of PL peaks seen in figure SI_3.

The effect seen due to addition of $PbCl_2$ is likely a result of suppression of PbI_4^{2-} by starving the film formation reaction of excess iodide during conversion to the perovskite phase combined with replacement of iodide with chloride in the coordination shells of highly coordinated lead species that form on perovskite surfaces [24, 38]. The slow reaction between S1- and S2- precursor left some unconverted S1-precursor in the film even up to 15% Cs. This phenomenon could be reduced by longer annealing time or adding more Cs. The full conversion was achieved at 20% Cs as confirmed by the XRD results shown in figure SI_4. Therefore, with the addition of 7% $PbCl_2$, up to 20% of Cs was incorporated into the film. One more advantage of $PbCl_2$ was improved uniformity of perovskite film thickness as depicted in figure SI_6 and SI_7.

The results were still not very repeatable, resulting with occasional frosty films under the same processing conditions. More repeatable glossy films were achieved by adding a short annealing (50 °C–1 min) step after the first spin coating step that allowed for consistently dry films. Thin films became

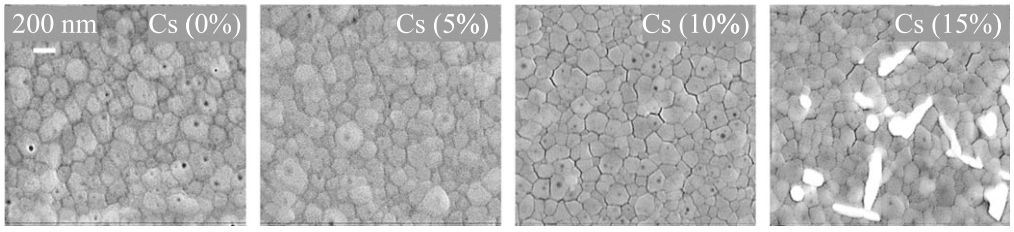

Figure 6. SEM image of the surface of perovskite films with varying Cs composition. (Scale bar is same for all images).

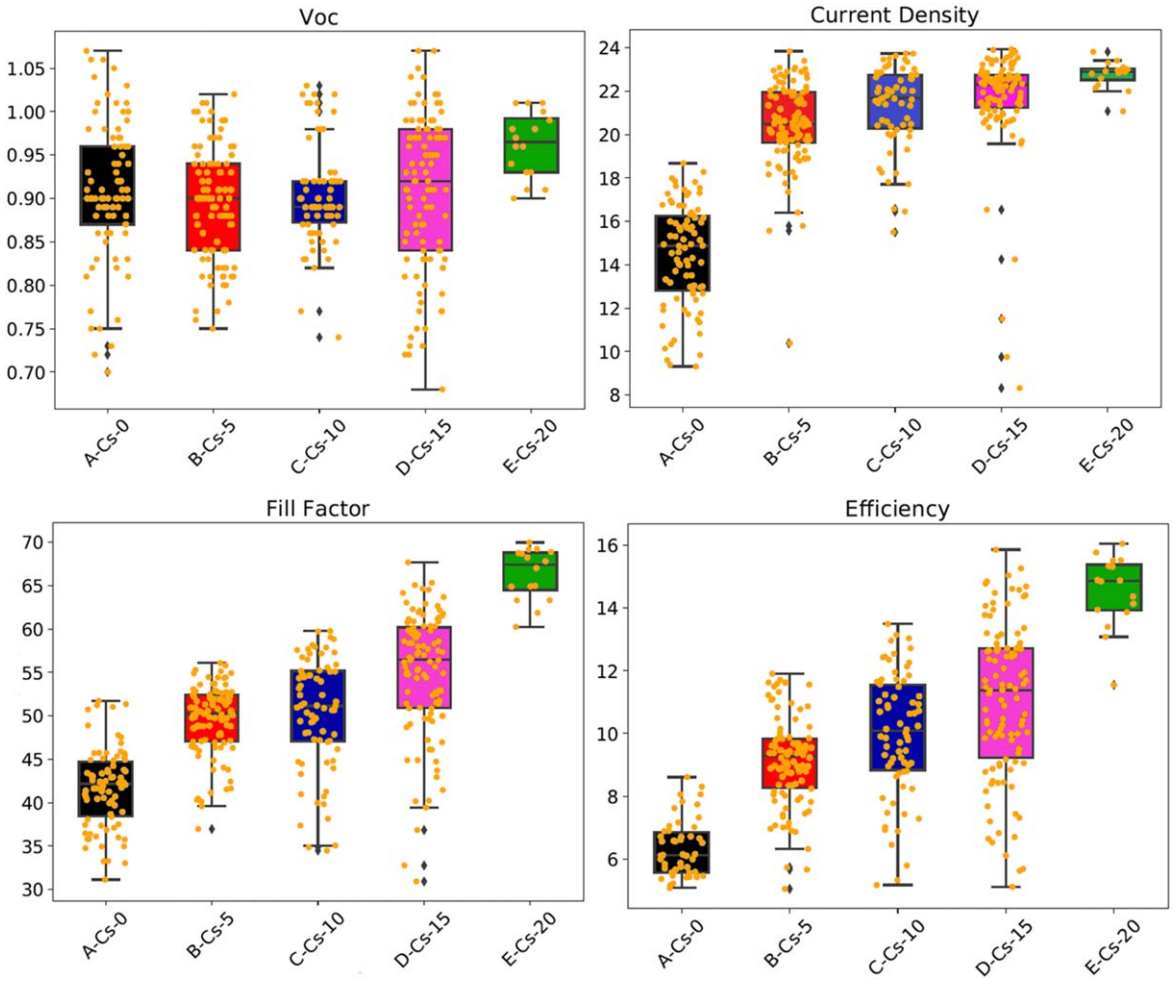

Figure 8. A box and whiskers plot of Open circuit voltage (V), Current density (J cm^{-2}), Fill factor (%) and Efficiency (%) of several batches of devices with Cs variation from 0% to 20%.

relatively dense after annealing, resulting in slower inter-diffusion in second step and leaving some portion of PbI_2 unconverted as seen from XRD in figure SI_5. However, the device's performance did not change on aggregate when compared between the annealed and not-annealed process. This showed that a reasonably small fraction of residual PbI_2 will not be detrimental to the device performance [39].

3.7. Device performance

The devices characteristics from several batches were combined to look at the big picture and a trend on how the added Cs content is affecting the device performance as shown in figure 8. The data contains all samples with and without $PbCl_2$. The data also contains samples with and without annealing the S1-precursor for any given Cs composition. For Cs-20%, however, it only contains data from the annealed S1-precursor mixed with $PbCl_2$.

The strongest correlation as expected can be seen in the current density (J_{SC}) and the fill factor (FF) of the devices. There is a sharp increase initially after introducing the Cs into the film followed by a steady increase with the increase in Cs content. This improvement is certainly due to the improvement in the absorption of the film, along with better charge collection by getting rid of excess PbI_2. The improved FF with increasing Cs incorporation can also be attributed to the absence of excess PbI_2. The excess PbI_2 contributes to a shunting path through the absorber and thus reduces the FF. However, it does not contribute to lowering the open circuit voltage (V_{oc}) because the improvement in PL in this case is mainly by the passivation of grain boundaries due to PbI_2 and not by the improvement in the absorber quality itself. The whole data set does not show any correlation of Cs concentration with the V_{OC} of the devices. A current–voltage characteristic of the set of highest efficiency devices among all the Cs variation is shown in figure 9. Both Cs-15% and Cs-20% reached a maximum efficiency of ~16%.

The effect on current collection due to the presence of residual PbI_2 at the bottom of the perovskite is clearly visible in the EQE of the devices shown in figure 10. In an inverted structure perovskite solar cell, light enters the device from the back side through the hole transporting layer (HTL)—NiO_x. The photons with the highest energy are absorbed first, thus the EQE response on the shorter wavelength side is dependent on the HTL/perovskite side of the device. The notch on the shorter wavelength side seen in figure 10 slowly disappears with the increase in Cs content. This disappearance of the

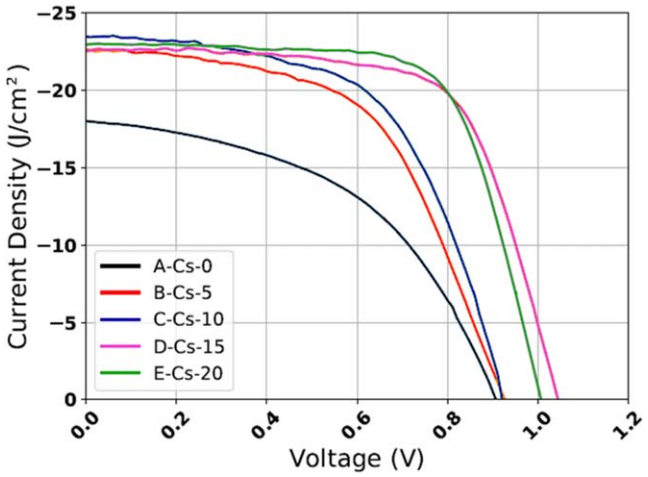

Figure 9. Current/Voltage characteristics of perovskite devices with varying Cs content.

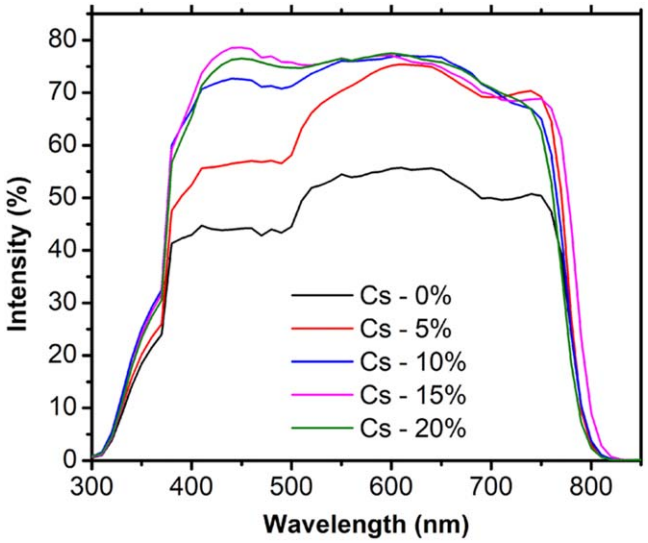

Figure 10. EQE of the perovskite devices with varying composition of Cs from 0% to 20%, showing the effect of PbI_2 at the perovskite/HTL interface.

notch is directly correlated with the content of the PbI_2 at the HTL/perovskite interface.

4. Conclusion

An inter-diffusion approach is used to incorporate Cs cations into FA/MA based perovskites that are currently one of the best reported photo-absorbers. The work done here showed that FA/MA based devices perform better with the addition of Cs. One of the major limitations seen for devices without Cs is the high presence of residual PbI_2. Though a small amount of PbI_2 is beneficial for grain boundary passivation, the amount of excess PbI_2 found in our devices with the chosen approach adversely affected device performance. With the addition of Cs, the perovskite became more absorbing and the amount of residual PbI_2 decreased significantly. Thus, the addition of Cs improved both the current density and fill factor of the resulting device. The addition of a small amount of $PbCl_2$ and short annealing after first spin coating step increased inclusion of Cs of up to 20%, forming smooth and glossy films. The added Cs brought repeatable high current density and fill factor, and the devices reached efficiencies on the order of ~16%. However, the corresponding improvement in V_{OC} was not observed. Understanding the low V_{OC}, which is somewhat common in inverted structure, needs to be further investigated.

Acknowledgments

This material is based upon work supported by the National Science Foundation under Grant Number 1751946. The authors would also like to acknowledge the SEM and XRD characterization support from the Analytical and Diagnostic Laboratory (ADL) of Binghamton University.

ORCID iDs

Tara P Dhakal https://orcid.org/0000-0003-0885-3254

References

[1] Jiang Q, Chu Z, Wang P, Yang X, Liu H, Wang Y, Yin Z, Wu J, Zhang X and You J 2017 Planar-structure perovskite solar cells with efficiency beyond 21% *Adv. Mater.* **29** 1703852
[2] Singh T, Miyasaka T, Singh T and Miyasaka T 2018 Stabilizing the efficiency beyond 20% with a mixed cation perovskite solar cell fabricated in ambient air under controlled humidity *Adv. Energy Mater.* **8** 1700677
[3] Yang W S *et al* 2017 Iodide management in formamidinium-lead-halide–based perovskite layers for efficient solar cells *Science* **356** 1376–9
[4] Pazos-Outo L M, Patrick Xiao T and Yablonovitch E 2018 Fundamental efficiency limit of lead iodide perovskite solar cells *Phys. Chem. Lett.* **9** 1703–11
[5] Snaith H J 2018 Present status and future prospects of perovskite photovoltaics *Nat. Mater.* **17** 372–6
[6] Correa-Baena J-P, Saliba M, Buonassisi T, Grätzel M, Abate A, Tress W and Hagfeldt A 2017 Promises and challenges of perovskite solar cells *Science* **358** 739–44
[7] Li Z, Yang M, Park J-S, Wei S-H, Berry J J and Zhu K 2016 Stabilizing perovskite structures by tuning tolerance factor: formation of formamidinium and cesium lead iodide solid-state alloys *Chem. Mater.* **28** 284–292
[8] Jeon N J, Noh J H, Kim Y C, Yang W S, Ryu S and Seok S I 2014 Solvent engineering for high-performance inorganic–organic hybrid perovskite solar cells *Nat. Mater.* **13** 897–903
[9] Sani F, Shafie S, Lim H N and Musa A O 2018 Advancement on lead-free organic-inorganic halide perovskite solar cells: a review *Materials* **11** 1–17
[10] Beal R E *et al* 2016 Cesium lead halide perovskites with improved stability for tandem solar cells *J. Phys. Chem. Lett.* **7** 746–51
[11] Docampo P, Ball J M, Darwich M, Eperon G E and Snaith H J 2013 Efficient organometal trihalide perovskite planar-

heterojunction solar cells on flexible polymer substrates *Nat. Commun.* **4** 2761
[12] Luo D *et al* 2018 Enhanced photovoltage for inverted planar heterojunction perovskite solar cells *Science* **360** 1442–6
[13] Meng L, You J, Guo T-F and Yang Y 2016 Recent advances in the inverted planar structure of perovskite solar cells *Acc. Chem. Res.* **49** 155–65
[14] Yan W, Ye S, Li Y, Sun W, Rao H, Liu Z, Bian Z and Huang C 2016 Hole-transporting materials in inverted planar perovskite solar cells *Adv. Energy Mater.* **6** 1–20
[15] Nejand B A, Gharibzadeh S, Ahmadi V and Reza Shahverdi H 2016 Novel solvent-free perovskite deposition in fabrication of normal and inverted architectures of perovskite solar cells *Sci. Rep.* **6** 1–14
[16] Sahli F and Werner J 2018 Fully textured monolithic perovskite/silicon tandem solar cells with 25.2% power conversion efficiency *Nat. Mater.* **17** 820–6
[17] Stoumpos C C, Malliakas C D and Kanatzidis M G 2013 Semiconducting tin and lead iodide perovskites with organic cations: phase transitions, high mobilities, and near-infrared photoluminescent properties *Inorg. Chem.* **52** 45
[18] Lee J-W *et al* 2015 Formamidinium and cesium hybridization for photo-and moisture-stable perovskite solar cell *Adv. Energy Mater.* **5** 1501310
[19] Jeon N J, Noh J H, Yang W S, Kim Y C, Ryu S, Seo J and Seok S I 2015 Compositional engineering of perovskite materials for high-performance solar cells *Nature* **517** 476–80
[20] Mcmeekin D P *et al* 2016 A mixed-cation lead mixed-halide perovskite absorber for tandem solar cells *Science* **351** 151–5
[21] Saliba M *et al* 2016 Incorporation of rubidium cations into perovskite solar cells improves photovoltaic performance downloaded from *Science* **354** 206–9
[22] Sun Y, Peng J, Chen Y, Yao Y and Liang Z 2017 Triple-cation mixed-halide perovskites: towards efficient, annealing-free and air-stable solar cells enabled by $Pb(SCN)_2$ Additive OPEN *Sci. Rep.* **7** 46193
[23] Saliba M *et al* 2016 Cesium-containing triple cation perovskite solar cells: improved stability reproducibility and high efficiency *Energy Environ. Sci.* **9** 1989–97
[24] Stewart R J, Grieco C, Larsen A V, Doucette G S and Asbury J B 2016 Molecular origins of defects in organohalide perovskites and their influence on charge carrier dynamics *J. Phys. Chem. C* **120** 12392–402
[25] Chen J, Xu J, Zhao C, Zhang B, Liu X, Dai S and Yao J 2019 Efficient planar heterojunction $FA_{1-x}Cs_x$ PbI_3 perovskite solar cells with suppressed carrier recombination and enhanced open circuit voltage via anion-exchange process *ACS Appl. Mater. Interfaces* **11** 4597–606
[26] Zhang Y, Shen Y, Xu Z, Chen Q, Zhou H, Zheng G, Zhou N and Li L 2017 CsI pre-intercalation in the inorganic framework for efficient and stable $FA_{1-x}Cs_xPbI_3$ (Cl) perovskite solar cells *Small* **13** 1700484
[27] Ray A, Qiu W, Gehlhaar R, Bastos J P, Cheyns D, Jaysankar M, Merckx T, Poortmans J and Heremans P 2017 An Interdiffusion method for highly performing cesium/formamidinium double cation perovskites *Adv. Funct. Mater.* **27** 1700920
[28] Zhang T, Yang M, Zhao Y and Zhu K 2015 Controllable sequential deposition of planar CH_3NH_3 PbI_3 Perovskite films via adjustable volume expansion *Nano Lett.* **15** 35
[29] Liu J, Shirai Y, Yang X, Yue Y, Chen W, Wu Y, Islam A and Han L 2015 High-quality mixed-organic-cation perovskites from a phase-pure non-stoichiometric intermediate $(FAI)_{1-x}$-PbI_2 for solar cells *Adv. Mater.* **27** 4918–23
[30] Harms H A, Etreault N T, Pellet N, El Bensimon M, Grätzel M and Grätzel G 2014 Mesoscopic photosystems for solar light harvesting and conversion: facile and reversible transformation of metal-halide perovskites *Faraday Discuss.* **176** 251–69
[31] Chen Q, Zhou H, Song T-B, Luo S, Hong Z, Duan H-S, Dou L, Liu Y and Yang Y 2014 Controllable self-induced passivation of hybrid lead iodide perovskites toward high performance solar cells *Nano Lett.* **14** 4158–63
[32] Liu F *et al* 2016 Is excess PbI_2 benefi cial for perovskite solar cell performance? *Adv. Energy Mater.* **6** 1502206
[33] Chan Kim Y *et al* 2016 Beneficial effects of PbI_2 incorporated in organo-lead halide perovskite solar cells *Adv. Energy Mater.* **6** 1502104
[34] Cao D H, Stoumpos C C, Malliakas C D, Katz M J, Farha O K, Hupp J T and Kanatzidis M G 2014 Remnant PbI_2, an unforeseen necessity in high-efficiency hybrid perovskite-based solar cells? *APL Mater.* **2** 091101
[35] Zhang T, Guo N, Li G, Qian X and Zhao Y 2016 A controllable fabrication of grain boundary PbI_2 nanoplates passivated lead halide perovskites for high performance solar cells *Nano Energy* **26** 50–6
[36] Saliba M, Correa-Baena J-P, Wolff C M, Stolterfoht M, Phung N, Albrecht S, Neher D and Abate A 2018 How to make over 20% efficient perovskite solar cells in regular (N−i−p) and inverted (P−i−n) architectures *Chem. Mater.* **30** 4193–201
[37] Yang W S, Noh J H, Jeon N J, Kim Y C, Ryu S, Seo J and Seok S I 2015 High-performance photovoltaic perovskite layers fabricated through intramolecular exchange *Science* **348** 1234–7
[38] Yu H, Wang F, Xie F, Li W, Chen J and Zhao N 2014 The role of chlorine in the formation process of '$CH_3NH_3PbI_{3-x}Cl_x$' perovskite *Adv. Funct. Mater.* **24** 7102–8
[39] Fisher D, Saouma F, Jang J and Dhakal T P 2016 The effect of grain improvement on carrier lifetime in perovskite solar devices *Conf. Record of the IEEE Photovoltaic Specialists Conf.* vol 2016 (https://doi.org/10.1109/PVSC.2016.7749707)